CrystEngComm

Bulk crystal growth and characterization of the bismuth ferrite-based material Bi3FeO4(MoO4)2

Journal:	*CrystEngComm*
Manuscript ID	CE-ART-12-2018-002137.R1
Article Type:	Paper
Date Submitted by the Author:	18-Feb-2019

Complete List of Authors:	Li, Conggang; Shandong University, State Key Laboratory of Crystal Materials Gao, Zeliang; Shandong University, State Key Laboratory of Crystal Materials Tian, Xiangxin; Shandong University, State Key Laboratory of Crystal Materials Zhang, Junjie; Materials Science and Technology Division, Oak Ridge National Laboratory, 1 Bethel Valley Rd. Oak Ridge, TN 37831 United States. Ju, Dianxing; Shandong University, State Key Laboratory of Crystal Materials Wu, Qian; Shandong University, State Key Laboratory of Crystal Materials Lu, Weiqun; Shandong University, State Key Laboratory of Crystal Materials Sun, Youxuan; Shandong University, State Key Laboratory of Crystal Materials Cui, De-Liang; State Key Lab of Crystal Materials, Tao, Xutang; Shangdong University, State Key Laboratory of Crystal Materials

Journal Name

ARTICLE

Bulk crystal growth and characterization of the bismuth ferrite-based material $Bi_3FeO_4(MoO_4)_2$

Received 00th January 20xx,
Accepted 00th January 20xx

DOI: 10.1039/x0xx00000x
www.rsc.org/

Conggang Li,[a] Zeliang Gao,[a] Xiangxin Tian,[a] Junjie Zhang,[a,b] Dianxing Ju,[a] Qian Wu,[a] Weiqun Lu,[a] Youxuan Sun*,[a], Deliang Cui[a] and Xutang Tao*,[a]

High-quality single crystals of the bismuth ferrite-based material $Bi_3FeO_4(MoO_4)_2$ sized up to 28 ×20 × 12 mm^3 were successfully grown via the modified top-seeded solution growth (TSSG) technique by using MoO_3-Bi_2O_3 self-flux. $Bi_3FeO_4(MoO_4)_2$ crystallizes into the space group *C*2/c (No.15, a = 16.927(12) Å, b = 11.672(12) Å, c = 5.263(4) Å, and Z =4) with a typical scheelite-type structure. The as-grown crystal exhibits major face forms {100}, {110}, and {111}, which is consistent with the predicted growth morphology on basis of the BFDH method. The high-resolution X-ray diffraction results demonstrate that the FWHM of the (200) face of the crystal is 31 arcsec, which indicates a high quality. The thermal measurements showed that the crystal melts incongruently and is thermally stable up to 912 °C. The crystal also displays a wide transmission region of 0.64–5.8 μm with a bandgap of 2.26 eV. Moreover, the magnetization properties with variations in temperature were measured, and the anti-ferromagnetic ordering is found to occur at 11K. Notably, the Raman scattering measurements show that the crystal exhibits an intense Raman shift and narrow line-width that are comparable with those of the YVO_4 crystal. In addition, first-principles calculations on the title compound were carried out to analyze the structure-property relationships. These results of the $Bi_3FeO_4(MoO_4)_2$ single crystals may provide a better understanding for further studies of these materials.

1. Introduction

Bismuth-based compounds have attracted much attention for long time owing to their critical importance in providing the key functions of magnetism, photocatalysis, ferroelectricity, semiconductivity, Raman shifts, laser host media and second order nonlinear frequency conversion.[1-4] Therefore, over the past decade, extensive research has been devoted to a variety of different derivatives of bismuth containing metal oxides.[5] As the typical Bi-based derivates, such as $BiFeO_3$, $Bi_2Fe_4O_9$ and $Bi_{25}FeO_{39}$, all of them exhibit a variety of intriguing phenomena due to their versatile structures favored by partially filled *d*-orbitals of Fe and the stereo-chemically active electron lone pair of Bi, particularly for the $BiFeO_3$, which is the only room-temperature magnetoelectric multiferroic material with the polarization and magnetization caused from Bi^{3+} and Fe^{3+}, respectively. [6-9] It was recently reported that these bismuth-based oxides are also considered as good substrates for composition tuning to tailor the structure and physical properties.[5] However, the preparation of pure bismuth ferrites, either polycrystals or single crystals, has been proved to be challenging mainly due to their peculiar thermodynamic characteristics, which hinders its further practical applications.

Bismuth molybdates/tungstates is another typical category of bismuth-based materials owing to their enrichment of the structural chemistry, especially for those exhibit the distinct structural features of intergrowth of fluorite-like $[Bi_2O_2]^{2+}$ sheets.[10,11] Octahedrally coordinated d^0 transition metals (Mo, W) exist that are susceptible to distortions in bismuth molybdate/tungstate, which is considered to be the driving force for a variety of technologically important optoelectronic properties.[12] The $[WO_x]$ and $[MoO_x]$ groups in the bismuth molybdates/tungstate are also contribute to the intensive Raman shifts, narrow linewidth, broad transmission spectra and stable physical-chemical properties, and further revealed the highly efficient Raman crystals of these materials.[13,14]

It is worth noting that combinations of the intrinsic functional properties in crystalline materials by incorporating different components with advanced structures are becoming more meritorious and intriguing; these combinations may offer new opportunities for the acquisition of specific properties and potential applications.[15,16] For example, the resultant $RbFe(MoO_4)_2$ exhibits new magnetic ferroelectric properties depending on the combination of Rb^+, Fe^{3+} element ions and $[MoO_4]$ groups.[17,18] The $BaTeMo_2O_9$ also shown the Raman and acousto–optic properties based on the intriguing merits of $BaMoO_4$ and TeO_2.[19-22] However, there is a notable absence of detailed investigations into the effects of combining bismuth ferrite with bismuth molybdate on the multifunctional properties.

Inspired by the above, we focused on a bismuth-based compound, namely, $Bi_3FeO_4(MoO_4)_2$ (BFM) by combining Bi^{3+}, Fe^{3+} element ions and $[MoO_4]$ groups with d^0 electronic configuration to maintain the attractive properties. BFM was first reported by Sleight et al.[23] in

[a]State Key Laboratory of Crystal Materials & Institute of Crystal Materials, Shandong University, No. 27 Shanda South Road, Jinan 250100, P. R. China.
[b]Materials Science and Technology Division, Oak Ridge National Laboratory, 1Bethel Valley Rd. Oak Ridge, TN 37831 United States.
E-mail: txt@sdu.edu.cn, yx.sun@sdu.edu.cn
Electronic supplementary information (ESI) available.

1974, where the powder product was synthesized. And then, Nie et al.[24] studied the surface characteristics of BFM with scanning electron microscopy (SEM) and transmission electron microscopy (TEM). Unfortunately, previous research was mainly focused on the polycrystalline forms and photocatalysts of BFM, and none have carried out the growth and properties of bulk BFM single crystals. Therefore, to obtain the intrinsic properties without grain boundary effects and make further progress in the investigation of their structure-property relationships and potential technological applications, the acquisition of BFM single crystals of high quality and large size would be highly desirable.

Here, we present the synthesis and, growth of bulk high-quality single crystals of BFM with dimensions of 28 mm × 20 mm × 12 mm via the modified top-seeded solution growth (TSSG) slow cooling technique. X-ray single-crystal diffraction experiments demonstrate that the target compound has a typical scheelite structure of space group *C*2/c. Additionally, the rocking curve, magnetic property, thermal stability and optical properties, as well as structure-physical property relationships are investigated in detail. These experimental observations are very valuable for further comprehension of the intrinsic properties and exploration of functional property combinations in these materials, which in turn extends the applications of these materials in photoelectric devices.

2. Experimental

2.1 Polycrystalline Synthesis

Polycrystalline samples for BFM were prepared through conventional high-temperature solid-state reaction. Stoichiometric amounts of MoO_3 (Alfa Aesar, 99.95%) and Fe_2O_3 (Alfa Aesar, 99.8%) and Bi_2O_3 (Shanghai Chemical Reagent Research Institute Co., Ltd., AR) were thoroughly ground together and then pressed into a pellet. The raw pellet was placed in an alumina crucible, gradually elevated to sintering temperatures of 720 °C and, held for 72 h in air with several intermittent grindings. Subsequently, the sample was slowly cooled to room temperature. Finally, the resultant yellow product was obtained.

2.2 Powder X-ray Diffraction (PXRD)

The purity of the resultant yellow product was checked by powder X-ray diffraction. The PXRD measurements were carried out at room temperature using a BrukerAXS D8 ADVANCE X-ray diffractometer provided with Cu Kα radiation (λ = 1.5418 Å) and the 2θ range was 10−80° with a step time of 0.4s and a step size of 0.02°.

2.3 DSC and TGA measurement

The thermal stability of the BFM was studied by using a TGA/DSC1/1600HT analyzer (Mettler Toledo Instruments). A powder sample prepared through grinding the single crystal was placed in a platinum crucible and heated at a rate of 5 K/min in the temperature ranging from 30 to 1000 °C under a flow of N_2 atmosphere.

2.4 Single Crystal Growth of BFM

In general, crystal growth in an open system has more flexibility for regulation of the conditions of growth and is more likely to grow large-sized, high-quality crystals. Single crystals of BFM were grown by the top-seeded solution growth (TSSG) slow cooling technique using MoO_3-Bi_2O_3 as the flux. Polycrystalline BFM was mixed thoroughly with MoO_3 and Bi_2O_3 at a molar ratio of BFM: MoO_3: Bi_2O_3 = 1: 5: 1. A platinum crucible containing the mixture was placed in the center of a vertical, temperature-controlled furnace and heated up to 950°C, held for 72h and stirred for 24 h to turn the mixture into a uniform solution. A platinum wire was introduced into surface of the solution at 860°C, and the temperature was decreased to 840°C at the rate of 1-5 °C/h. Small crystals nucleated on the platinum wire, from which high-quality crystals were selected to be BFM seed crystals after several cycles of seed cultivation and selection. Subsequently, the TSSG method was employed, and the exact saturation point was determined to be 845 °C by distinguishing the dissolution and growth of the seed crystals on the surface of the solution. At 850 °C, a selected seed with a high quality and regular shape was slightly introduced into the melt and held for 2 hours to eliminate the impurities on the seed crystal surface. Then, the solution was cooled to the saturation temperature quickly in 30 min and then cooled to 832 °C at a slow rate of 0.5-1 °C/day while the seed crystal rotated at 25 rpm. When the growth process was complete, the crystal was hung over the solution and then cooled to room temperature at a rate of 100−150 °C/day.

2.5 Single-Crystal X-ray Diffraction

A BFM crystal with dimensions of approximately 0.10 × 0.08 × 0.07 mm^3 was selected for structure determination. Single-crystal X-ray diffraction data was recorded using graphite-monochromated Mo Kα radiation (λ = 0.71073 Å) on a Bruker SMART APEX-II diffractometer equipped with a CCD area. The preliminary lattice parameters were determined according to three sets of frames. Using the APEX2 software,[25] data integration and cell refinement were implemented. Multi-scan absorption corrections were applied by using the SCALE program for the area detector. The structure of the BFM crystal was determined using the software SHELX with direct methods. The atoms in the structure were refined using anisotropic thermal parameters. All the calculations were implemented with the SHELXTL crystallographic software package.[26,27] The details of crystallographic data are given in Table S1.

2.6 High-resolution X-ray Diffraction Measurements

High-resolution X-ray diffraction (HRXRD) was performed by a Bruker-AXS D5005HR diffractometer provided with a four-crystal Ge (220) monochromator with Cu-Kα radiation (λ = 1.54056 Å). A BFM [200] oriented wafer with dimensions of 6 × 6 × 2 mm^3 was mechanically polished on both sides and was used as the sample.

2.7 Density and Hardness Measurements

The density of the BFM crystal was determined by the Archimedes method at room temperature. The density was calculated according to $\boldsymbol{\rho_{exp} = m_0\rho_{water}/(m_0 - m_1)}$, in which $\boldsymbol{m_0}$ is the weight of the sample in air, $\boldsymbol{m_1}$is the weight the sample soaked in distilled water, and $\boldsymbol{\rho_{water}}$=0.998g cm^{-3}.[28] The density was confirmed by averaging the results of several repetitions of the entire process.

The mechanical hardness of the BFM crystal was estimated using a DHV-1000 micro-hardness tester with a loading time of 10 s and an indentation of 50 g. Three thin polished (100), (010) and (001)-faced wafers were employed as test samples, and five test points in different locations were measured on each sample to obtain an average value. The Mohs hardness (H_M) and micro-hardness(H_V) values were calculated by the following equations:[29]

$$\boldsymbol{H_V = 1.8544 \times (P/d^2)}\ \text{kg·mm}^{-2} \quad (1)$$

$$\boldsymbol{H_M = 0.675 \times (H_V)^{1/3}} \quad (2)$$

where *P* denotes the load pressure, and *d* denotes the corresponding diagonal length of the indentations on the sample surface.

2.8 Linear Optical Measurements

The UV−visible diffuse reflectance measurements of the BFM powder prepared through grinding the single crystal were performed by a Shimadzu UV 2550 spectrophotometer equipped with an integrating sphere in the spectral range of 200−800 nm, which provided the UV-or-visible cut off edge. $BaSO_4$ was used as a

standard sample. Then, the reflectance spectra were converted to absorbance by using the Kubelka−Munk function.[30] To further explore the accurate transparency region of the BFM, optical transmittance spectra for BFM at room temperature were also collected with a Hitachi U-4100 UV−vis−IR spectrometer in the ranging of 400−2000 nm and a Nicolet NEXUS 670 FTIR spectrometer in the range of 2000 to 8000 nm, respectively. One 1.0 mm thick wafer perpendicular to the (100) face of the BFM crystal polished on both sides was used as a test sample.

2.9 Magnetic properties

The magnetic properties were performed using a Quantum Design MPMS 3 SQUID magnetometer (superconducting quantum interference device, Quantum Design Inc.). The applied magnetic field was set at 1000 Oe, and the variable temperature range was 5 - 300 K. The powder of the BFM single crystal was measured after being thoroughly ground and soaked in diluted hydrochloric acid for several hours.

2.10 Spontaneous Raman Spectra

One square wafer of BFM crystal, perpendicular to crystallographic axis [001] was cut from an as-grown BFM crystal, and mechanically polished on both sides as the test sample. Raman spectral measurements were taken for the BFM sample at room temperature by a JY-HR 800 Raman spectrometer with a backscattering scheme in the range of 100-1200 cm^{-1} using 1064 nm radiation as the pump source.

2.11 Computational Descriptions

The electronic structure and optical properties were investigated using the CASTEP,[31] a total energy package based on plane-wave pseudopotential method utilizing density functional theory (DFT). The generalized gradient approximation (GGA)[32] with the Perdew−Burke−Ernzerhof (PBE) functional[33] was adopted during the calculation. Single-crystal structural data of BFM was used for the theoretical calculations.

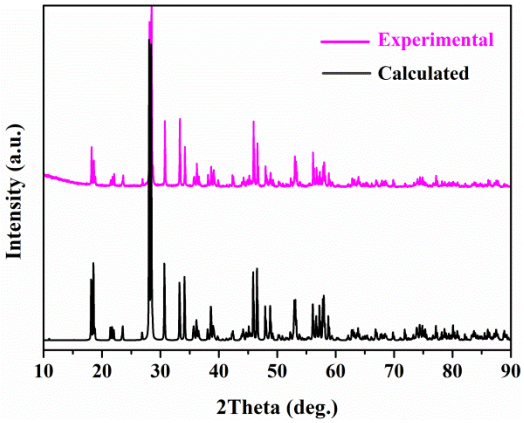

Figure 1. Calculated and experimental powder X-ray diffraction patterns of BFM polycrystalline.

3. Results and discussions

3.1 Synthesis and Characterization of Polycrystalline BFM

Polycrystalline samples of BFM were obtained by standard solid-state reaction techniques. The resultant yellow-brown product was checked by XRD analysis. As shown in Figure 1, the experimental data agree well with the pattern calculated from the single crystal structure data of BFM using the computer program Mercury 3.3. To characterize the thermal stability of the BFM crystal, TGA and DSC were performed, and the corresponding results are shown in Figure 2. It was worth nothing that there was only one endothermic peak in the DSC heating curve at 912 °C and no obvious weight loss in the TGA curve, implying that BFM potentially melts congruently. However, the PXRD data of the residue after DSC and TGA undoubtedly confirmed the crystal decomposed into $Bi_2Mo_3O_{12}$ and other unknown phase (Figure S1), which demonstrated that BFM melts incongruently. Therefore, large BFM single crystals can only be grown below the decomposition temperature through the flux method.

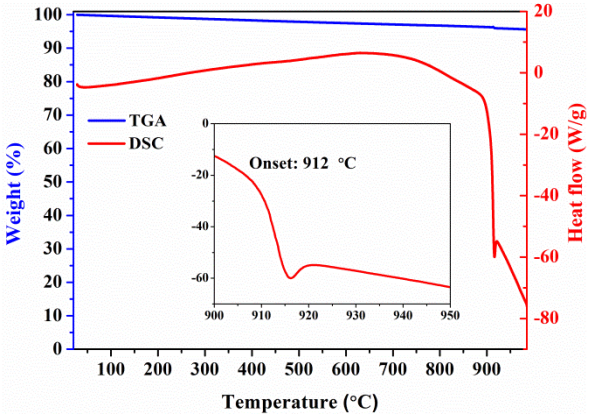

Figure 2. TGA and DSC data for the BFM crystal. The extrapolated onset temperature is marked.

3.2 Growth and Morphology of the BFM Crystals

The growth of bismuth ferrite-based oxide crystals has been challenging because of the high crystallization temperature. The flux growth method is particularly preferable as this method enables growth of crystal at a temperature well under the melting point of the target solution. Meanwhile, BFM melts incongruently, therefore, several circles of growth experiments were run in our laboratory.[34] To determine the suitable flux system, self-flux of MoO_3 was first employed to grow large BFM owing to the ability of this material to dissolve oxides. Nevertheless, the significant volatility of MoO_3 prevented the growth of large, high quality BFM crystals because of the very high crystallization temperature. Figure S2 showed the as grown BFM crystal which contained inclusions of flux. On basis of the phase diagram for the pseudobinary system MoO_3-Bi_2O_3, there is a eutectic point approximately 620 ℃ when the molar percent of Bi_2O_3 is approximately 16%.[35] On the other hand, according to previous study, Bi_2O_3 fluxes have a significantly reduced volatility.[36] Therefore, the MoO_3-Bi_2O_3 mixture was considered to be suitable for the growth of BFM single crystal. After many tries, the good and appropriate molar ratio of BFM: Bi_2O_3: MoO_3 was determined for the growth of BFM single crystals. Based on above optimized experimental growth conditions, certain BFM crystals with regular morphology were grown through spontaneous nucleation during the slow-cooling process shown in Figure 3a. Subsequently, high-quality single crystals of sizes up to 28 mm × 20 mm × 12 mm were successfully grown using [100]-oriented seed through the TSSG method with MoO_3-Bi_2O_3 as flux. Figure 3c shows that the as-grown crystal has a well-developed shape with no visible cracks or inclusions. According to the Bravais-Friedel and Donnay-Harker (BFDH) method,[37] the theoretical morphologys of BFM crystals were also calculated as shown in Figure 3b and 3d, respectively. As presented in Figure 3d, the crystal grown with a [100]-oriented seed clearly exhibits {100}, {110} and {111} facets, which matches well with the experimental results. The X-ray rocking curve is an effective way to evaluate the perfection of crystals, which can provide information on the quality of different zones of the crystals. To determine the crystal quality, rocking curve measurements were carried out. The full-width at half-maximum (FWHM) of the rocking curve of the (200) wafer was estimated to be 31 arcsec (Figure 4),

which indicated the as-grown crystal is of high quality and is sufficient for the measurements of the intrinsic physical properties.

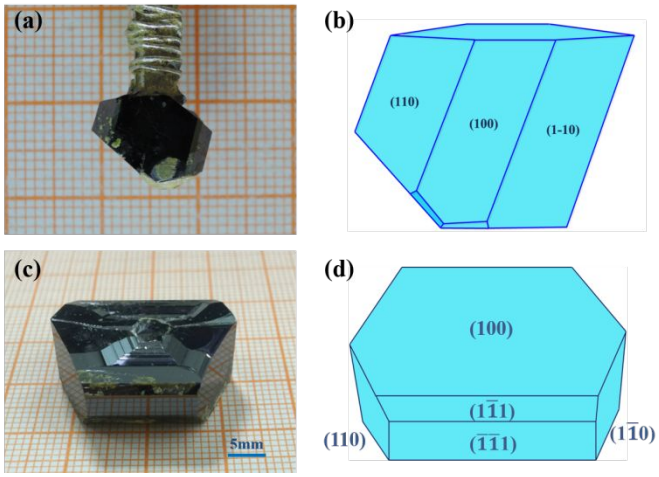

Figure 3. (a) and (b) Photographs of BFM crystals grown through spontaneous nucleation along the platinum wire and the corresponding calculated morphology of the BFM crystal. (c) and (d) High-quality bulk single crystal grown using [100]-oriented seed and the corresponding morphology of the BFM crystal.

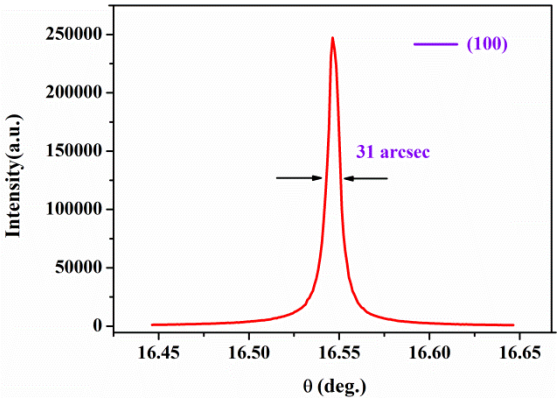

Figure 4. Rocking curve for the BFM single crystal. The acute and symmetric rocking curves demonstrate that the as-grown BFM crystal is of high quality.

3.3 Hardness and Density

It has been well established that the anisotropic hardness of a crystal has a direct effect on the mechanical processing and the application of the material.[29] The H_V hardness values determined using a micro-hardness tester on the (100), (010) and (001) planes of the BFM crystal were calculated to be 536.0, 582.8 and 540.5 kg mm^{-2}, respectively, corresponding to Mohs hardness values of 5.48, 5.64 and 5.50, respectively (Table. 1). As Figure S3 illustrates, the indentation morphologies of the material faces are rhombic and regular, which means that the results are reasonable. The results show that the hardness exhibits a relatively anisotropy among the three different directions of the BFM crystal and are slightly higher than those of certain d^0 transition metal molybdates crystals.[28] This result also confirms that the BFM crystal has excellent stability, which is beneficial in processing and further application. The average density of the pure BFM crystal at room temperature was determined to be 7.128g/cm^3 using the Archimedes method, which is consistent with the calculated value (7.131 g/cm^3) using the crystal structure.

Table 1. H*v* hardness and Mohs hardness of BFM crystal.

Crystal planes	(100)	(010)	(001)
H_V (kg/mm^2)	536.0	582.8	540.5
H_M	5.48	5.64	5.50

3.4 Crystal Structure

The structure of BFM has been reported by Sleight et al.[23,24,38] To provide better insights into the relationship between crystal structure and physical property, crystal structure was investigated using single-crystal X-ray diffraction techniques. BFM crystallizes in a monoclinic crystal system with a centrosymmetric space group of *C*2/c. The crystallographic data and structural refinement parameters for BFM single crystal are listed in Table S2. The information on the crystal structure of BFM is also given in Figure 5. Considering the wide variation in Bi-O bond lengths, bond valence sums (BVS)[39] of the cations were calculated to evaluate the contribution of each oxygen atom to the bond valence and are presented in Table 2, showing that the contributions of the longer bonds are weaker and indicating good rationality for the structure. Unit cell, ball-and-stick and polyhedral representations of the BFM are displayed in Figure 5b-5d, respectively. As described above, both Bi1-O and Bi2-O are in asymmetric coordination environments attributable to the distortions of the lone-pair of the Bi^{3+} derived from second-order Jahn-Teller (SOJT) distortions, which can result in a local dipole moment. Nevertheless, based on our structure refinements of BFM, there exists an inversion center for the distributions of these asymmetric polyhedra that generates a centrosymmetric *C*2/c space group. The typical scheelite-type structure plays a key role in generating a host of intriguing properties and promising potential applications in various fields for this material.

3.5 Optical Properties

To shed light on the optical properties of BFM, the UV-vis diffuse reflectance spectrum was obtained as presented in Figure 6. Near the optical transmission cutoff, the band gap, absorption and wave frequency correspond to the following equation,[40]

$$\alpha h\nu = A(h\nu - E_g)^{n/2}$$

According to the band structure calculation, BFM has an indirect band gap, so n = 4 for BFM. The $(\alpha h\upsilon)^{1/2}$-$(h\upsilon)$ curve is also listed in Figure 6a. The bandgap was calculated to be 2.26 eV, which is a narrower band energy than that of $BiVO_4$.[41] To further confirm the accuracy of the value for the absorption cut-off edge, the UV-vis-NIR and mid-IR transmission spectra of the BFM crystals were obtained at room temperature by using a 4mm × 4mm × 1mm crystal wafer. As illustrated in Figure 6b, BFM exhibits a wide range of transmittance from approximately 640 nm to 5800 nm, which is comparable to those of previously reported bismuth molybdates.

3.6 Magnetic Properties

Iron molybdates are expected to exhibit intriguing magnetic properties depending on the connectivity and dimensionality between the molybdates and the Fe^{3+}.[42] To gain insight into the magnetic properties of BFM, the magnetization-temperature (M-T) curve was determined, as presented in Figure 7. Figure 7a shows that one distinct peak is observed at approximately 11 K, indicating the establishment of antiferromagnetic ordering. A similar situation also occurs in those of $La_3Fe(MoO_4)_6$ as recently reported.[43] On the other hand, the magnetization-field curve presents a straight line crossing the origin of the coordinates, and the value of the magnetization is above 0 and far less than 1 (Figure 7b), which evidenced a paramagnetic behavior at 200K.

Journal Name

ARTICLE

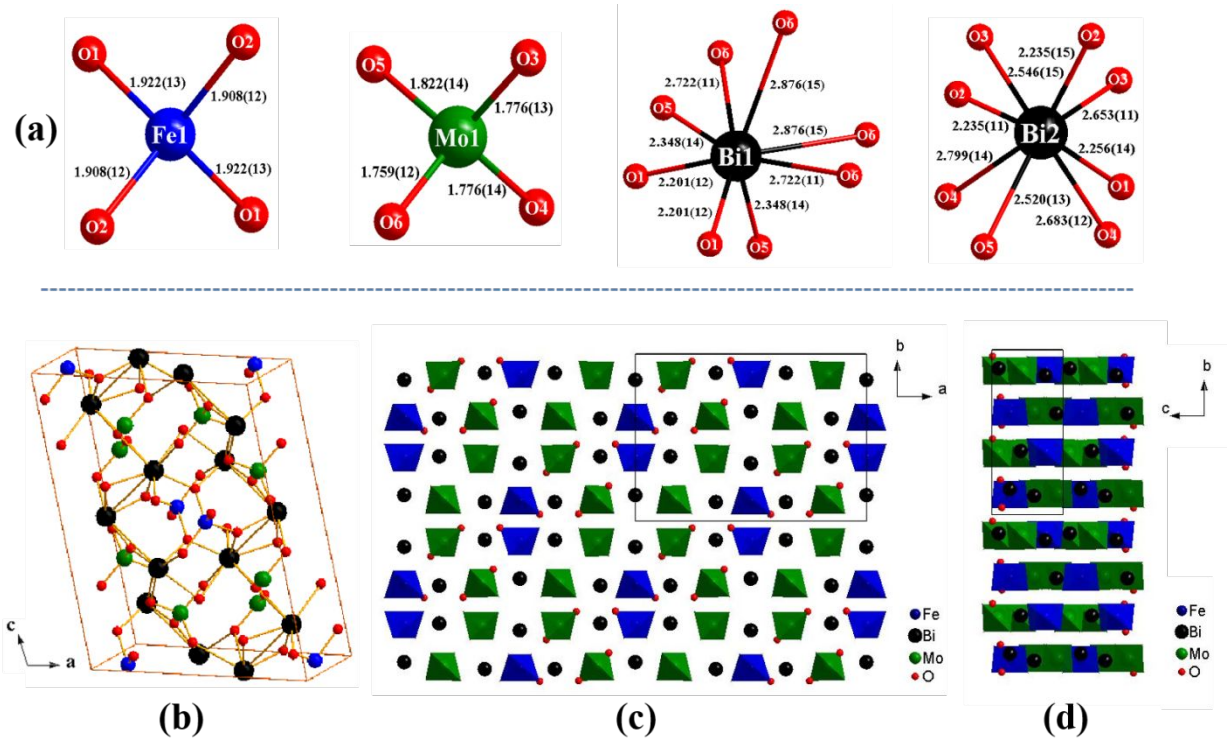

Figure 5. (a) Ball and stick diagrams of the FeO_4 tetrahedral, MoO_4 polyhedral, $Bi1O_8$ polyhedral and $Bi2O_8$ polyhedral geometries, respectively, in the structure of BFM; (b) The coordination environments of the unit cell for the BFM crystal structure along the *b*-axis; (c) and (d) polyhedral representations of the BFM with scheelite-type structure in the *ab*- and *bc*-planes, respectively.

Table 2. Main interatomic distances (Å) and corresponding bond valences of BiO_8 polyhedron in $Bi_3FeO_4(MoO_4)_2$

$Bi(1)O_8$ polyhedron			**$Bi(2)O_8$ polyhedron**		
bond	d_{Bi-O}	V_{ij}	bond	d_{Bi-O}	V_{ij}
Bi1-O1	2.201	0.741	Bi2-O2	2.235	0.676
Bi1-O1	2.201	0.741	Bi2-O2	2.235	0.676
Bi1-O5	2.348	0.498	Bi2-O1	2.256	0.638
Bi1-O5	2.348	0.498	Bi2-O5	2.52	0.313
Bi1-O6	2.722	0.181	Bi2-O3	2.546	0.292
Bi1-O6	2.722	0.181	Bi2-O3	2.653	0.218
Bi1-O6	2.876	0.120	Bi2-O4	2.683	0.201
Bi1-O6	2.876	0.120	Bi2-O4	2.799	0.147
Σ_{Vij}		3.08	Σ_{Vij}		3.161

Journal Name

ARTICLE

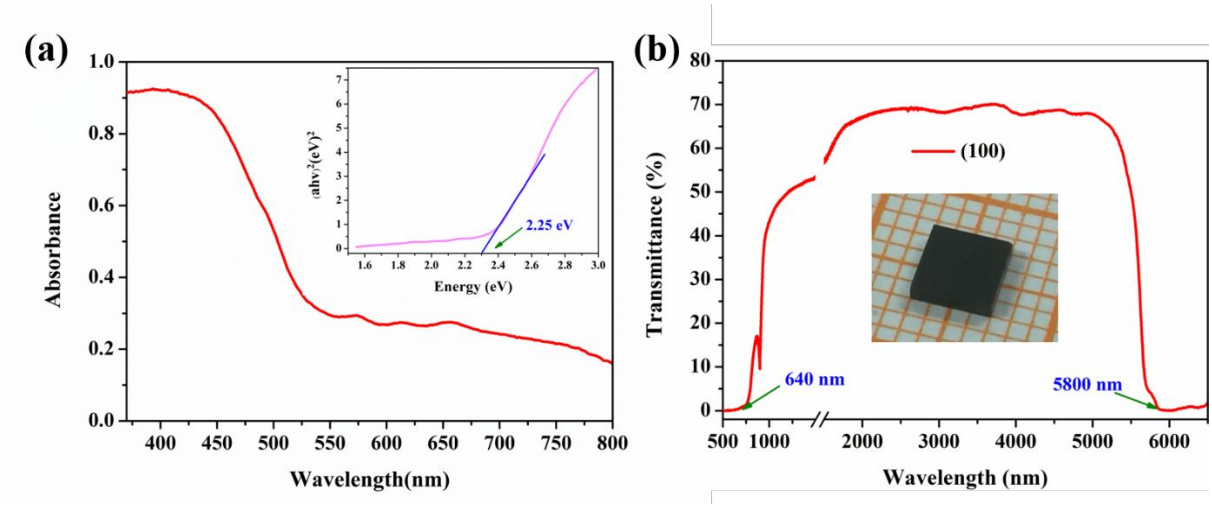

Figure 6. (a) UV-vis diffuse reflectance spectrum for BFM, the inset represents the $(\alpha hv)^{1/2}$–(hv) curve. (b) The transmittance of the BFM single crystal perpendicular to the (100) face.

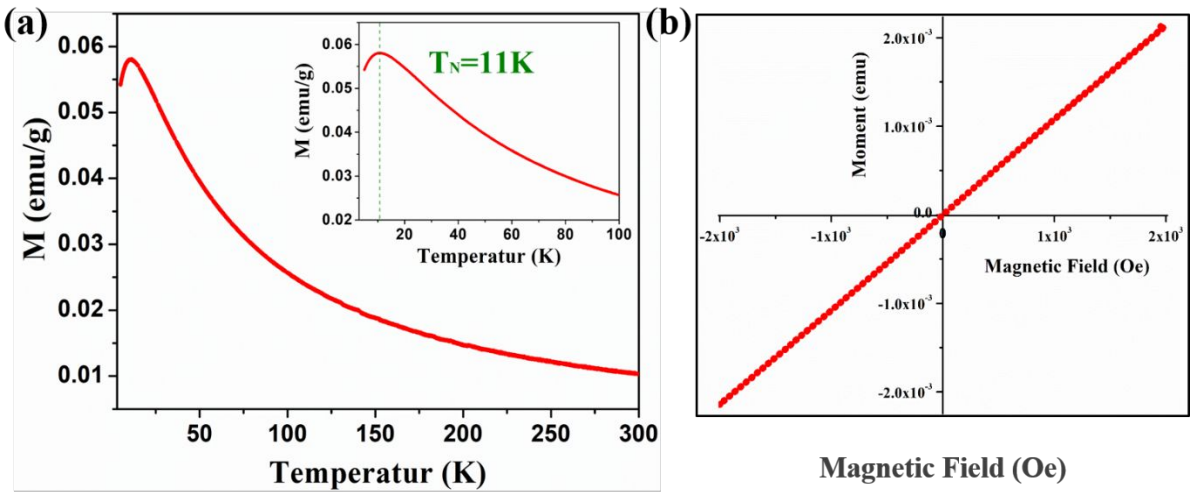

Figure 7. (a) Temperature dependence of the magnetization for the BFM single crystal under a magnetic field of 1000 Oe. (b) Magnetization as a function of field of BFM single crystal at 200 K.

3.7 Raman Spectra

Raman spectroscopy is an effective characterization tools for probing the coordination geometry of inorganic oxide compounds.[44] In 1983, Grzybowska et al. reported the spectroscopic properties of BFM using polycrystalline powders. In present study, the polarized Raman properties of BFM are investigated systematically from the point of view of single crystal. Moreover, the polarization spectrum is beneficial to the analysis of vibration modes which has anisotropy, and on this basis, the prospect of its Raman application is also properly evaluated.[45] The analysis of the Raman spectrum of the BFM was implemented by comparison with other Raman spectra from the existing crystals that were previously studied.

As Figure 8a illustrates, polarized Raman spectra of the BFM single crystal along the *Z*-axis in different polarization configurations ranging from 100 to 1200 cm^{-1} were measured. The observed Raman peaks and shoulders assigned are listed in Table S3. The strongest Raman shifts at 868.67 cm^{-1} and sub-strongest peaks at 124.49 cm^{-1} were determined for the Z(XX)Z polarizations, whereas weaker Raman shifts were observed for several other polarizations Z(YY)Z, Z(XY)Z and Z(YX)Z. The Raman shifts observed in BFM with different polarization configurations show distinct anisotropy that may be bound up with the vibrations of anionic groups in the structure of the BFM crystal. According to early investigations,[46] the 868.67 and 870.41cm^{-1} bands are unambiguously assigned to stretching vibrations of the short Mo-O bonds, whereas the 610-790

cm^{-1} bands are derived from stretching vibrations of Mo-O bonds and Mo-O-Bi bridges. The modes below 200 cm^{-1} were attributed to stretching vibrations of the Bi-O bands and translational motions of Bi^{3+} and Mo^{6+} cations. Based on previous data in the literature, the stretching vibrations of Bi-O bonds, bending vibrations of Mo-O bonds and translations of iron atoms give rise to many bands in the 200-600 cm^{-1} range.

The Raman gain is a considerable indicator that determines the Stokes threshold and conversion efficiency for a Raman laser medium. To further investigate the Raman scattering and evaluate its potential application, comparison measurements for both BFM and Raman crystal YVO_4 were carried out as presented in Figure 8b. The polarized Raman spectrum along the Z-axis measured in the Z(XX)Z polarization configurations exhibit almost the same or even stronger Raman intensity compared with that of YVO_4. Moreover, molybdate generally has a high refractive index and a high density of vibrational scattering centers, which is essential to achieving a high Raman gain. Therefore, BFM may be as outstanding of a Raman crystal as YVO_4.

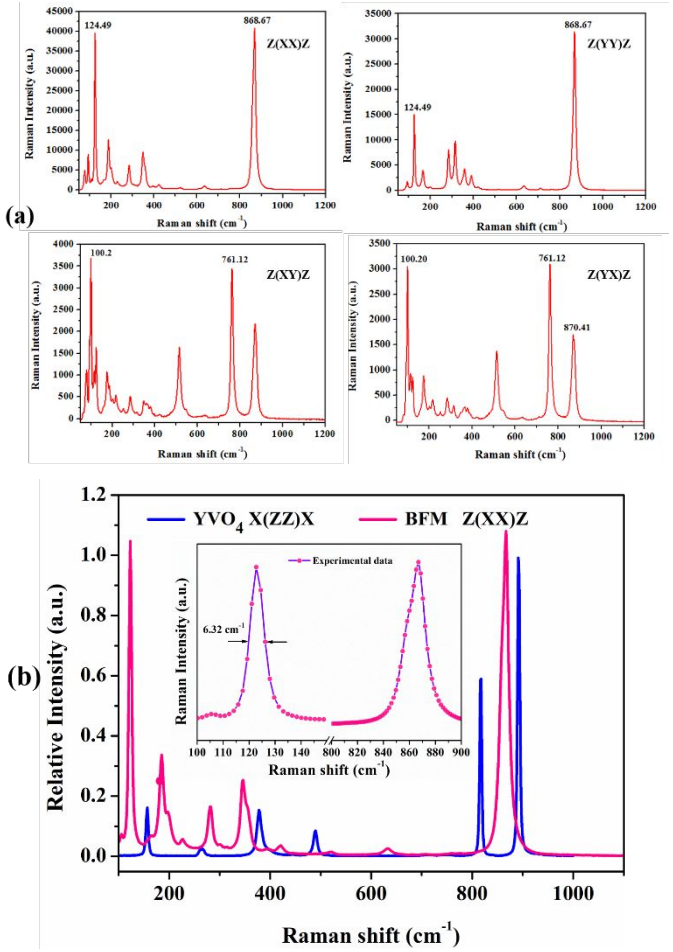

Figure 8. (a) Room temperature polarized Raman spectrum for the BFM single crystal along the *Z*-axis with different scattering geometry projects. (b) Relative polarized spontaneous Raman scattering spectra of YVO_4 and BFM crystals at room temperature.

3.8 Electronic Structure Calculation.

Physical properties are generally closely related to the structures.[47] To gain further insights into the electronic properties, band structure and DOS calculations of BFM were also carried out by the total-energy code CASTEP according to density functional theory (DFT). The calculated band structure of BFM along high symmetry points at the first Brillouin zone is shown in Figure 9a, where the highest valence band (VB) is located near the M point, while the bottom of the conduction band (CB) occurs along the L point. Therefore, BFM has an indirect band gap of 2.14 eV, which is slightly lower than the experimental value of 2.26 eV determined from the visible absorption edge. The different values for the band gaps from the experiment and calculations are due to the limitations of DFT methods. Meanwhile, the total density of states (TDOS) and partial density of states (PDOS) of the BFM crystal are also presented in Figure 9b. The valence bands in the lower energy range from −25.0 to −15.0 eV comprise O-2s, Bi-5d and small amounts of Mo-4d states. The region ranging from approximately -10 to -7.5 eV is dominated by Bi-6s with small amounts of O-2p and Fe-3d states. The VBs from - 7.0 to 0 eV are mainly attributed to the O-2p, Mo-4d and Fe-3d states with small amounts of Fe-3p and Mo-4p. The band above the Fermi level also mainly originates from the O-2p, Mo-3d, and Fe-3d states and small amounts of Mo-3p, Fe-3p and Bi-3p. Therefore, we can propose that the optical properties of BFM crystal are attributed to the collective action of the MoO_4, FeO_4 and BiO_8 polyhedra.

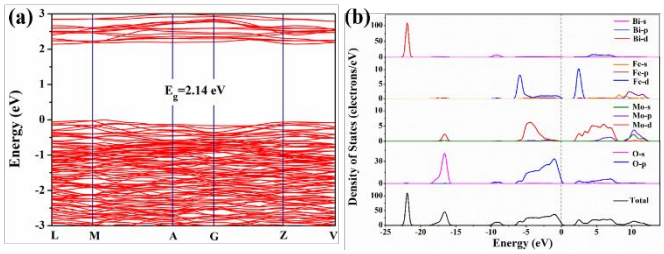

Figure 9. Electronic structure of BFM. (a) Energy band structure. (b) TDOS and PDOS curves. The Fermi level is set at 0.0 eV.

4. CONCLUSION

In summary, large BFM single crystals of sizes up to 28 × 20 × 12 mm^3 were cultivated by the top-seeded solution method for the first time. Rocking curve measurements show a FWHM of 31 arcseconds for the (200) reflection indicting a high-quality crystal. BFM shows a typical scheelite-type structure and crystallizes in the central space group C2/c (No. 15) with cell parameters a = 16.927(12) Å, b = 11.672(12) Å, c = 5.263(4) Å, and Z = 4. The thermal characterization of the BFM crystal demonstrates that it is highly stable up to 912 °C and melts incongruently. The optical transmittance spectrum of BFM exhibits a wide transmission range from 640 nm to 5.8 μm with an indirect bandgap of 2.26 eV. Moreover, the antiferromagnetic property has been highlighted for the first time, and the magnetic phase transition occurs at approximately T_N=11 K. More importantly, the BFM single crystal also exhibits intense Raman shift and narrow line-width, which indicates that the BFM crystal is a promising material in Raman frequency conversions. These behaviors may provide better understanding for the further study of these materials.

Conflicts of interest

There are no conflicts to declare.

Acknowledgements

This research is financially supported by the Shandong Provincial Key R&D Program, (2018CXGC0411), National Natural Science Foundation of China (Grant Nos. 51772170, 51572155 and 11504389), Young Scholars Program (2018WLJH67), National key Research and Development Program of China (2016YFB1102201), the Fundamental Research Founds of Shandong University (2017JC044) and the 111 Project 2.0 (Grant No: BP2018013). This research has been supported in part by ORNL Post-Doctoral

Development Fund by UT-Battelle, LLC under Contract No. DE-AC05-00OR22725 with the US Department of Energy.

Notes and references

1. G. Catalan and J. F. Scott, *Adv. Mater.*, 2009, **21**, 2463-2485.
2. V. A. Khomchenko, D. V. Karpinsky and J. A. Paixão, *J. Mater. Chem. C*, 2017, **5**, 3623-3629.
3. X. Tian, Z. Gao, F. Chen, Q. Wu, C. Li, W. Lu, Y. Sun and X. Tao, *CrystEngComm*, 2018, **20**, 2669-2680.
4. F. Gao, Q. Lu and S. Komarneni, *Chem. Commun*., 2005, **4**, 531-533.
5. J. Wu, Z. Fan, D. Xiao, J. Zhu and J. Wang, *Prog. Mater. Sci*., 2016, **84**, 335-402.
6. J. Wang, J. B. Neaton, H. Zheng, V. Nagarajan, S. B. Ogale, B. Liu, D. Viehland, V. Vaithyanathan, D. G. Schlom5, U. V. Waghmare, N. A. Spaldin, K. M. Rabe, M. Wuttig and R. Ramesh, Science., **2003**, 299, 1719-1722.
7. J. Ma, J. Hu, Z. Li and C. W. Nan, *Adv. Mater*., 2011, **23**, 1062-1087.
8. D. Lebeugle, D. Colson, A. Forget, M. Viret, P. Bonville, J.F. Marucco and S. Fusil, *Phys. Rev. B*, 2007, **76**, 024116.
9. A. Perejón, E. Gil-González, P. E. Sánchez-Jiménez, A. R. West and L. A. Pérez-Maqueda, *J. Eur. Ceram. Soc*, 2019, **39**, 330-339.
10. N. A. Benedek, J. M. Rondinelli, H. Djani, P. Ghosez and P. Lightfoot, *Dalton Trans.*, 2015, **44**, 10543-10558.
11. C. Kongmark, R. Coulter, S. Cristol, A. Rubbens, C. Pirovano, A. Löfberg, G. Sankar, W. van Beek, E. Bordes-Richard and R.-N. Vannier, *Cryst. Growth Des*., 2012, **12**, 5994-6003.
12. P. S. Halasyamani, *Chem. Mater*., 2004, **16**, 3586.
13. T. T. Basiev, A. A. Sobol, Y. K. Voronko and P. G. Zverev, *Opt. Matter.,* 2000, **15**, 205.
14. X. Tian, Q. Wu, P. Zhao, Z. Wang, X. Feng, C. Li, Y. Sun, S. Wang, Z. Gao and X. Tao, *CrystEngComm*, 2015, **17**, 4525-4532.
15. M. Wu and X. C. Zeng, *Nano Lett*., 2016, **16**, 3236-3241.
16. X. Liu, P. Long, X. Wang, Z. Gao, Y. Lü and Z. Yi, *J. Mater. Chem. C*, 2017, **5**, 3238–3246.
17. J. S. White, C. Niedermayer, G. Gasparovic, C. Broholm, J. M. S. Park, A. Y. Shapiro, L. A. Demianets, and M. Kenzelmann, *Physical Review B*, 2013, **88**, 060409.
18. K. Cao, R. D. Johnson, F. Giustino, P. G. Radaelli, G. C. Guo and L. He, *Physical Review B*, 2014, **90**, 024402.
19. Z. L. Gao, S. D. Liu, S. J. Zhang, W. G. Zhang, J. L. He and X. T. Tao, *Appl. Phys. Lett*., 2012, **100**, 261905
20. Q. Wu, Z. Gao, X. Tian, X. Su, G. Li, Y. Sun, S. Xia, J. He and X. Tao, *Opt. Express*., 2017, **25**, 24893-24900.
21. C. G. Li, X. X. Tian, Z. L. Gao, Q. Wu, P. Zhao, Y. X. Sun, C. Q. Zhang, S. J. Zhang, D. L. Cui and X. T. Tao, *Cryst. Growth Des*., 2018, **18**, 3376–3384.
22. Q. Wu, Z. Gao, H. Wang, C. Li, W. Lu, X. Tian, Y. Sun, N. Lin, S. Xia and X. Tao, *Cryst. Growth Des*., 2018, **18**, 5054-5062.
23. A. W. Sleight and W. Jeitschko, *Mater. Res. Bull*., 1974, **9**, 951.
24. X. Nie, W. Wulayin, T. Song, M. Wu and X. Qiao, *Appl. Surf. Sci*., 2016, **387**, 351.
25. Bruker *APEX2*, Bruker AXS, Inc., Madison, WI, 2005.
26. G. M. Sheldrick, *SHEXTL version 6.12,* Bruker AXS, Inc., Madison, WI, 2001.
27. G. M. Sheldrick, *Acta Crystallogr. A*, 2008, **64**, 112-122.
28. C. Li, Z. Gao, X. Tian, Q. Wu, F. Liu, X. Du, D. Huang, Y. Sun, D. Cui and X. Tao, *J. Alloy. Comp.*, 2019, **777**, 59-66.
29. Q. Hu, Z. Jia, C. Tang, N. Lin, J. Zhang, N. Jia, S. Wang, X. Zhao and X. Tao, *CrystEngComm*, 2017, 19, 537.
30. P. Kubelka and F. Z. Munk, *Tech. Phys*., 1931, **12**, 593–603.
31. S. J. Clark, M. D. Segall, C. J. Pickard, P. J. Hasnip, M. J. Probert, K. Refson and M. C. Payne, *Z. Kristallogr*., 2005, **220**, 567–570.
32. J. P. Perdew, K. Burke and M. Ernzerhof, *Phys. Rev. Lett*., 1996, **77**, 3865–3868.
33. J. P. Perdew, A. Ruzsinszky, G. I. Csonka, O. A. Vydrov, G. E. Scuseria, L. A. Constantin, X. Zhou and K. Burke, *Phys. Rev. Lett*., 2008, **100**, 136406.
34. B. Q. Zhao, L. Bai, B. X. Li, S. G. Zhao, Y. G. Shen, X. F. Li, Q. R. Ding, C. M. Ji, Z. S. Lin and J. H. Luo, *Cryst. Growth Des*., 2018, **18**, 1168−1172.
35. T. Chen and G. S. Smith, *J. Solid State Chem*.,1975, **13**, 288-297.
36. D. E. Bugaris and H. C. zur Loye, Angew. Chem., *Int. Ed. Engl*., 2012, **51**, 3780.
37. J. D. H. Donnay and D. Harker, *Am. Mineral*., 1937, **22**, 446–467.
38. W. Jeitschko, A. W. Sleight, W. R. McClellan and J. F. Weiher, *Acta Crystallogr., Sect. B: Struct. Crystallogr. Cryst. Chem*., 1976, **B32**, 1163.
39. N. E. Brese and M. O'Keeffe, *Acta Crystallogr. Sect. B*, 1991, **47**, 192-197
40. P. Zhao, H. J. Cong, X. X. Tian, Y. X. Sun, C. Q. Zhang, S. Q. Xia, Z. L. Gao and X. T. Tao, *Cryst. Growth Des*., 2015, **15**, 4484–4489.
41. X. Liu, F. Zhang, P. Long, T. Lu, H. Zeng, Y. Liu, R. L. Withers, Y. Li and Z. Yi, *Adv. Mater*., 2018, **30**, 1801619.
42. A. V. Sobolev, E. S. Kozlyakova, I. S. Glazkova, V. A. Morozov, E. A. Ovchenkov, O. S. Volkova, A. N. Vasiliev, N. S. Ovanesyan, Y. M. Kadyrova, E. G. Khaikina, K. Molla, B. Rahaman, T. Saha-Dasgupta, S. Kamusella, H.-H. Klauss and I. A. Presniakov, *J. Phys. Chem. C*, 2018, **122**, 19746-19755.
43. C. Kongmark, R. Coulter, S. Cristol, A. Rubbens, C. Pirovano, A. Lofberg, G. Sankar, W. V. Beek, E. B. Richard and R. N. Vannier, *Cryst. Growth Des*., 2012, **12**, 5994–6003.
44. Z. Zhang, X. Tao, J. Zhang, Y. Sun, C. Zhang and B. Li, *CrystEngComm*, 2013, **15**, 10197.
45. B. Grzybowska, E. Payen, L. Gengembre, and J. P. Bonnelle, *Bull. Pol. Acad. Sci*. 1983, **31**, 245.
46. J. J. Zhang, Z. H. Zhang, W. G. Zhang, Q. X. Zheng, Y. X. Sun, C. Q. Zhang and X. T. Tao, *Chem. Mater*., 2011, **23**, 3752–3761.
47. C. Li, Z. Gao, X. Tian, Q. Wu, W. Lu, Y. Sun and X. Tao, *CrystEngComm*, 2018, **20**, 5602-5608.

Table of Contents Entry

Bulk crystal growth and characterization of bismuth ferrite-based material $Bi_3FeO_4(MoO_4)_2$

Conggang Li,[a] Zeliang Gao,[a] Xiangxin Tian,[a] Junjie Zhang,[a,b] Dianxing Ju,[a] Qian Wu,[a] Weiqun Lu,[a] Youxuan Sun*,[a], Deliang Cui[a] and Xutang Tao*,[a]

[a]State Key Laboratory of Crystal Materials, Shandong University, Jinan 250100, P. R. China.

[b]Materials Science and Technology Division, Oak Ridge National Laboratory, 1 Bethel Valley Rd. Oak Ridge, TN 37831 United States.

E-mail: txt@sdu.edu.cn; yx.sun@sdu.edu.cn

The large high-quality $Bi_3FeO_4(MoO_4)_2$ single crystals sized up to 28 ×20 × 12 mm^3 were grown sucsessfully by TSSG method. The thermal, optical, magnetization and polarized Raman properties are investigated in detail.